One-loop corrections to the bubble nucleation rate at finite temperature

J. Baacke*and V. G. Kiselev†
Institut für Physik, Universität Dortmund, D-44221 Dortmund, Germany
(Received 19 August 1993)

We present an evaluation of the one-loop prefactor in the lifetime of a metastable state which decays at finite temperature by bubble nucleation. Such a state is considered in the one-component φ^4 model in three space dimensions. The calculation serves as a prototype application of a fast numerical method for evaluating the functional determinants that appear in semiclassical approximations.

PACS number(s): 98.80.Hw, 03.70.+k, 05.30.−d, 64.60.Qb

I. INTRODUCTION

The decay of metastable states by bubble nucleation appears in a large variety of physical contexts. It has received the attention of particle physicists and cosmologists due to its possible role in the evolution of the Universe. Since bubble formation is a basic mechanism in the kinetics of a first-order phase transition a precise determination of its rate is of prime importance. The semiclassical approach to bubble formation has been developed by Langer [1, 2] and Coleman and Callan [3, 4]. The leading factor in the transition rate is determined by the classical Euclidean trajectory. Quantum corrections may however modify the rate in a significant way. Their evaluation for a realistic model in three space dimensions is an enterprise that can easily reach the limits of practical computability. It is therefore very useful to have a method that leads to a fast numerical algorithm.

We will develop here such a method using as a simple model the four-dimensional φ^4 theory at finite temperature T given by the Euclidean action

$$S(\varphi)=\int_0^{1/T}d\tau\int d^3x\left[\tfrac{1}{2}\left(\partial_\mu\varphi\right)^2+U(\varphi)\right]. \tag{1.1}$$

The field potential $U(\varphi)$ is assumed to have two nondegenerate minima $\varphi_-=0$ and $\varphi_+>0$ (Fig. 1).

Any state built on the local minimum φ_- is metastable. Its decay rate per unit volume $\gamma=\Gamma/V$ at sufficiently high temperature is dominated by the energy $E=ST$ of a fluctuation which looks like a bubble $\phi(x)$ of the ϕ_+ phase. This bubble is in unstable equilibrium between collapse and unbounded expansion. The tree-level approximation determines the order of magnitude of the decay rate as $\gamma\approx\exp\{-E(\phi(x))/T\}$.

Fluctuations around the critical bubble contribute a preexponential factor to the decay rate which is known to take the form [1, 2]

$$\gamma=\frac{\omega_-}{2\pi}\left(\frac{E(\phi)}{2\pi T}\right)^{3/2}|\mathcal{D}|^{-1/2}\exp\left\{-\frac{E(\phi)}{T}-S_{\rm ct}\right\} \tag{1.2}$$

to one-loop accuracy. The coefficient $\mathcal{D}$ here reads

$$\mathcal{D}(T)=\frac{\det'[-(\partial/\partial\tau)^2-\Delta+U''(\phi)]}{\det[-(\partial/\partial\tau)^2-\Delta+U''(0)]}. \tag{1.3}$$

The prime in the determinant implies omitting of three zero modes in it. The temperature dependence of $\mathcal{D}$ arises from imposing periodic boundary conditions in the time direction with a period $1/T$. $\mathcal{D}(T)$ as introduced in Eq. (1.3) is ill defined because of ultraviolet divergences. As discussed in [4] they are absorbed by the counterterm action $S_{\rm ct}$ which has been introduced in the exponent. It will be specified below.

As we have mentioned above we will present here a fast method for evaluating the fluctuation determinant (1.3). The method which we are going to use is based on a well-known theorem [5] that is formulated and proven in an elegant way in Appendix A of Coleman's 1977 Erice Lectures [6]. It was also used some time ago in analytical calculations of the determinant (1.3) in (1+1)-dimensional space in the thin-wall approximation [7, 8] and in Ref. [9]. What is new here is application of that idea to a sys-

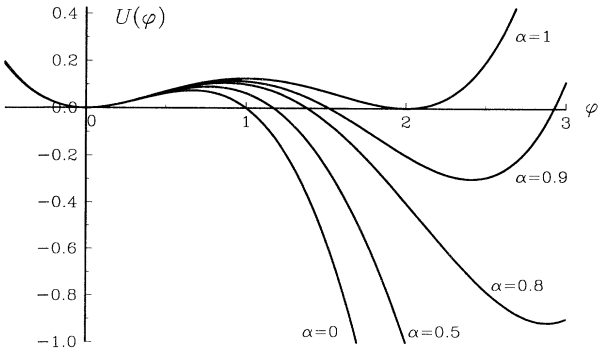

FIG. 1. Potential $U(\varphi)$ in (2.1). It is plotted in dimensionless form which enters the integral (2.2). The curves are labeled with the value of α.

*Electronic address: baacke@het.physik.uni-dortmund.de
†On leave of absence from Institute of Physics, 220602 Minsk, Byelorussia. Electronic address: kiselev@het.physik.uni-dortmund.de

tem in three dimensions, the elaboration of a numerical method, and the discussion of regularization and renormalization.

We decompose fluctuations around $\phi(x)$ into partial waves, calculate the ratio of determinants J_l of radial operators, using the theorem mentioned above, and, finally, obtain $\ln \mathcal{D}$ as $\sum_l (2l+1) \ln J_l$.

In calculating $\ln \mathcal{D}$ we exclude the divergent perturbative contributions of first and second order in the external field created by the critical bubble. The regularized values of these contributions are then added analytically. All divergences of $\ln \mathcal{D}$ appear in the standard zero-temperature tadpole and fish diagrams.

This paper is organized as follows. In the next section we specify the form of the potential, write the equation for the critical bubble, and present our numerical results for $E(\phi)$. In Sec. III we describe the calculation of the regularized fluctuation determinant (1.3). A possible renormalization scheme is applied to the result in Sec. IV.

II. THE TREE-LEVEL ENERGY

In this section we discuss classical properties of the critical bubble. The generic one-component ϕ^4 potential reads

$$U(\varphi) = \frac{1}{2} m^2 \varphi^2 - \eta \varphi^3 + \frac{1}{8} \lambda \varphi^4 . \tag{2.1}$$

We choose the same dimensionless variables as in Ref. [10]: namely, $\mathbf{x} = \mathbf{X}/m$, $\tau = u/m$, $\varphi = \frac{m^2}{2\eta}\Phi$. The energy of a time-independent fluctuation then takes the form

$$E(\varphi) = \frac{m^3}{4\eta^2} \int d^3X \left(\frac{1}{2} (\nabla \Phi)^2 + \frac{1}{2}\Phi^2 - \frac{1}{2}\Phi^3 + \frac{\alpha}{8}\Phi^4 \right), \tag{2.2}$$

where

$$\alpha = \frac{\lambda m^2}{2\eta^2} . \tag{2.3}$$

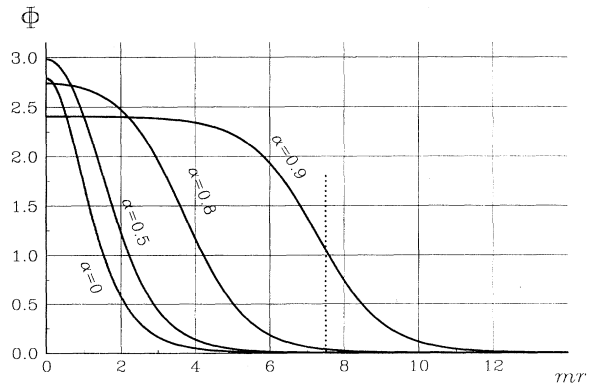

FIG. 2. The bubble-profile functions $\Phi(R)$ in units defined after Eq. (2.1) at $\alpha = 0.1,\ 0.5,\ 0.8,\ 0.9$. The radius of the thin-walled bubble $mr_{\rm TW} \approx 3/[4(1-\alpha)]$ is marked with a dashed line for $\alpha = 0.9$.

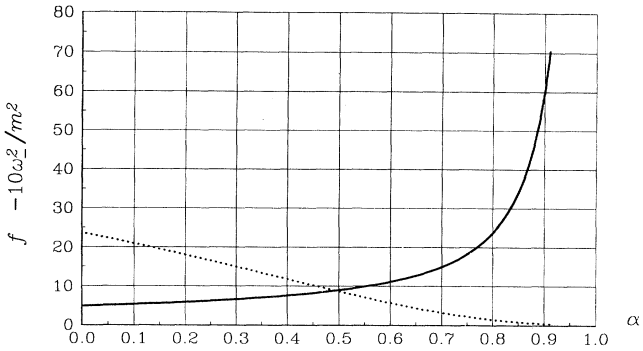

FIG. 3. The values of $f(\alpha)$ in (2.5) (solid line) and $-10\underline{\omega}^2/m^2$ (dotted line) vs α.

The limit $\alpha \to 1$ corresponds to the thin-wall approximation.

The critical bubble is a spherically symmetrical stationary point of E (2.2) obeying a dimensionless Euler-Lagrange equation

$$\frac{d^2\Phi}{dR^2} + \frac{2}{R}\frac{d\Phi}{dR} - \Phi + \frac{3}{2}\Phi^2 - \frac{1}{2}\Phi^3 = 0 \ . \tag{2.4}$$

We have solved this equation using the shooting method. The profiles $\Phi(R)$ are shown in Fig. 2 for some values of the parameter α .

We parametrize the value of E in the same way as in Ref. [10]:

$$E = \frac{4.851\ m^3}{\eta^2}\ f(\alpha). \tag{2.5}$$

The function $f(\alpha)$ is plotted in Fig. 3.

III. CALCULATION OF THE FLUCTUATION DETERMINANT

In this section we discuss a method of computing the ratio of functional determinants (1.3), which is based on earlier papers [7–9]. The explicit form of the operator in the nominator (1.3) is

$$-\frac{\partial^2}{\partial \tau^2} - \Delta + m^2 + V(r) \tag{3.1}$$

with the periodical boundary conditions for the eigenfunctions $\Psi(\tau, \mathbf{x}) = \Psi(\tau + 1/T, \mathbf{x})$. The space-dependent part V (3.1) of $U''(\phi)$ (1.3) reads

$$V(r) = U''(\Phi) - m^2 = -6\eta\phi(r) + \frac{3}{2}\lambda\phi^2(r) \ . \tag{3.2}$$

The free operator in the denominator (1.3) takes the same form as (3.1), but with $V(r) = 0$.

The time independence and spherical symmetry of the background bubble field yield a classification of ω^2_{n,l,n_r}, the eigenvalues of (3.1), with respect to the number n of their Matsubara frequencies $\nu = 2\pi n T$, radial quantum number n_r, and angular momentum l. One can formally

write the ratio of determinants (1.3) as

$$\mathcal{D}(T) = \prod_{n=-\infty}^{\infty} \prod_{l=0}^{\infty} \prod_{n_r=0}^{\infty} \left[\frac{\omega_{n,l,n_r}}{\omega^{(0)}_{n,l,n_r}} \right]^{2l+1} \tag{3.3}$$

with $\omega^{(0)}_{n,l,n_r}$ standing for the free eigenvalues.

The outline of our calculation is as follows. We compute first (Sec. III A) for each partial wave the product over n_r, i.e., the ratio of the determinants of the radial operators

$$J_l(\nu) = \frac{\det H_{\nu,l}}{\det H^{(0)}_{\nu,l}}, \tag{3.4}$$

here

$$H_{\nu,l} = -\frac{d^2}{dr^2} - \frac{2}{r}\frac{d}{dr} + \nu^2 + m^2 + V(r) \tag{3.5}$$

and $H^{(0)}_{\nu,l}$ has the same form, but without $V(r)$.

As the next step we calculate the product over l:

$$F(\nu) = \sum_{l=0}^{\infty} (2l+1) \ln J_l(\nu) \tag{3.6}$$

(Sec. III B). The function $F(\nu)$ is the sum of all three-dimensional one-loop one-particle-irreducible diagrams.

In terms of this function the final result reads

$$\ln \mathcal{D}(T) = \sum_{n=-\infty}^{\infty} F(2\pi n T) \quad . \tag{3.7}$$

This expression is formal because of the ultraviolet divergences in it. We first evaluate $\ln \mathcal{D}$ without the divergent part which is then accounted for in Sec. III C.

A. Determinants of the radial operators

In order to find $J_l(\nu)$ (3.4) we make use of a known theorem [5, 6] whose statement is

$$\frac{\det H_{\nu,l}}{\det H^{(0)}_{\nu,l}} = \lim_{r\to\infty} \frac{\psi_{\nu,l}(r)}{\psi^{(0)}_{\nu,l}(r)} \quad . \tag{3.8}$$

Here $\psi_{\nu,l}$ and $\psi^{(0)}_{\nu,l}$ are solutions to equations

$$H_{\nu,l}\psi_{\nu,l} = 0, \quad H^{(0)}_{\nu,l}\psi^{(0)}_{\nu,l} = 0 \tag{3.9}$$

and have the same regular behavior at $r = 0$. More exactly, the boundary conditions at $r = 0$ must be chosen in such a way that the right-hand side of Eq. (3.8) tends to 1 at $\nu \to \infty$.

It is convenient [11] to introduce a function $h(r)$ such as

$$\psi_{\nu,l} = [1 + h_l(r)] i_l(\kappa r), \quad h(0) = 0 \tag{3.10}$$

when $\psi^{(0)}_{\nu,l}$ is chosen here to be a spherical Bessel function

$$i_l(\kappa r) = \left(\frac{2\pi}{\kappa r}\right)^{1/2} I_{l+\frac{1}{2}}(\kappa r) \ , \quad \kappa(\nu)^2 = \nu^2 + m^2 \quad . \tag{3.11}$$

Therefore, by theorem (3.8), the ratio of determinants (3.4) can be expressed as

$$J_l(\nu) = [1 + h_l(\infty)] \quad . \tag{3.12}$$

In terms of the h function the first equation (3.9) reads

$$\left[\frac{d^2}{dr^2} + 2\left(\frac{i_l'(\kappa r)}{i_l(\kappa r)} m + \frac{1}{r}\right)\frac{d}{dr}\right] h_l(r) = V(r)[1 + h_l(r)] \quad . \tag{3.13}$$

It is worth considering the structure of a perturbation expansion

$$h_l(r) = \sum_{k=1}^{\infty} h_l^{(k)}(r) \tag{3.14}$$

in powers of the potential $V(r)$. This entails an analogous expansion for the ratios $J_l(\nu)$ in the sense that $J_l^{(k)} = h_l^{(k)}(\infty)$. The k-order contribution $h_l^{(k)}$ obeys an equation

$$\left[-\frac{d^2}{dr^2} + 2\left(\frac{i_l'(\kappa r)}{i_l(\kappa r)} m + \frac{1}{r}\right)\frac{d}{dr}\right] h_l^{(k)}(r) = V(r) h_l^{(k-1)}(r), \tag{3.15}$$

$h_l^{(0)} = 1$. The same equation is valid when $h_l^{(k)}$ are replaced by $h_l^{\overline{(k)}} = \sum_{q=k}^{\infty} h_l^{(q)}$. In this notation $h_l = h_l^{\overline{(1)}}$. A Green's function that gives the solution to Eq. (3.15) in the form

$$h_l^{\overline{(k)}}(r) = -\int_0^{\infty} dr' r'^2 G_l(r, r') V(r') h_l^{\overline{(k-1)}}(r') \tag{3.16}$$

with the right boundary condition at $r = 0$ reads

$$G_l(r, r') = \kappa \left(i_l(\kappa r_<) k_l(\kappa r_>) \frac{i_l(\kappa r')}{i_l(\kappa r)} - i_l(\kappa r') k_l(\kappa r') \right). \tag{3.17}$$

Here $r_< = \min\{r, r'\}$, $r_> = \max\{r, r'\}$, and

$$k_l(z) = \left(\frac{2}{\pi z}\right)^{1/2} K_l(z) \quad . \tag{3.18}$$

The first term on the right-hand side of Eq. (3.17) does not contribute to $h_l^{(k)}(\infty)$. The Green's function (3.17) gives rise to connected graphs as well as disconnected ones (Fig. 4). The latter are canceled in $\ln[1 + h_l(\infty)]$ whose expansion in k-order connected graphs $J_{l\ \mathrm{con}}^{(k)}(\kappa)$ reads

$$\ln J_l(\nu) = \ln[1 + h_l(\infty)] = \sum_{k=1}^{\infty} \frac{(-1)^{k+1}}{k} J_{l\ \mathrm{con}}^{(k)}(\nu) \quad . \tag{3.19}$$

This formula is analogous to the expansion of the full functional determinant in terms of Feynman diagrams

$$\ln \mathcal{D}(T) = \sum_{k=1}^{\infty} \frac{(-1)^{k+1}}{k} A^{(k)}(T) \quad . \tag{3.20}$$

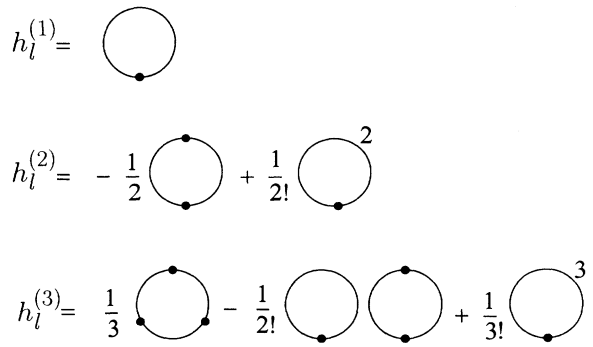

FIG. 4. The structure of the first $h_l^{(k)}(\infty)$. The solid line represents the last term in the Green's function (3.17). Dots stand for $V(r)$.

Here $A^{(k)}(T)$ is the one-loop Feynman graph of order k in the external potential $V(|\mathbf{x}|)$.

Indeed, it is obvious from Eq. (3.16) that $h_l^{(k)}$ and, therefore, $J_{l\ \mathrm{con}}^{(k)}$ are of the order V^k. Since the expansion of $\ln \mathcal{D}$ in powers of V is unique, we conclude that

$$A^{(k)}(T) = \sum_{n=-\infty}^{\infty} \sum_{l=0}^{\infty} (2l+1) J_{l\ \mathrm{con}}^{(k)}(2\pi n T) \quad . \tag{3.21}$$

One can verify this relation explicitly by expanding the propagator in $A^{(k)}$ as

$$\int \frac{d^3p}{(2\pi)^3} \frac{e^{i\mathbf{p}(\mathbf{x}-\mathbf{y})}}{p^2+m^2+\nu^2}$$

$$= \kappa \sum_{l=0}^{\infty} (2l+1) i_l(\kappa|\mathbf{x}|) k_l(\kappa|\mathbf{y}|) P_l\left(\frac{\mathbf{x}\cdot\mathbf{y}}{|\mathbf{x}||\mathbf{y}|}\right) \tag{3.22}$$

and performing the integration over all angular variables in the x representation.

It is not difficult to check, making use of a uniform asymptotic expansion of the modified Bessel functions in (3.17), that $J_{\mathrm{con}}^{(k)} \sim 1/l^k$ as $l \to \infty$. That results in the expected quadratic and logarithmic ultraviolet divergences in $\ln \mathcal{D}$ due to the contribution of $h^{(1)}(\infty)$ and $h^{(2)}(\infty)$. We have computed numerically $\ln \mathcal{D}^{\overline{(3)}}$ which is the sum (3.20) without first- and second-order diagrams $A^{(1)}$ and $A^{(2)}$. It reads explicitly

$$\mathcal{D}^{\overline{(3)}}(T) = \sum_{n=-\infty}^{\infty} F^{\overline{(3)}}(2\pi n T)$$

$$= \sum_{n=-\infty}^{\infty} \sum_{l=0}^{\infty} (2l+1) \left[\ln J_l(\nu)\right]^{\overline{(3)}} \quad , \tag{3.23}$$

where

$$\left[\ln J_l(\nu)\right]^{\overline{(3)}} = \left\{ \ln\left[1+h_l(\infty)\right] - h_l^{(1)}(\infty) - \left[h_l^{(2)}(\infty) \frac{1}{2} \left(h_l^{(1)}(\infty)\right)^2\right] \right\} . \tag{3.24}$$

The terms in square brackets here correspond to the fish diagram $J_{l\ \mathrm{con}}^{(2)}$ (Fig. 4). Since all contributions to $\ln \mathcal{D}^{\overline{(3)}}$ are ultraviolet finite, we need no regularization in computing them. The divergent contributions of the first and second order in V will be considered in Sec. III C.

We have determined $h_l(r)$ as solutions of Eq. (3.13), and $h_l^{\overline{(2)}}(r)$ as that of Eq. (3.15) by Nystrom's method. The values of $h_l^{(1)}(\infty)$, $h_l^{\overline{(2)}}(\infty)$, $h_l^{\overline{(3)}}(\infty)$ have been evaluated by performing integration (3.16). Only the last term in the Green's function (3.17) contributes here since $r \to \infty$. The ratio of $h_l^{\overline{(2)}}(\infty)$ found via differential equation (3.15) to that calculated as the integral (3.16) has been used to control the accuracy. In order to avoid numerical subtraction that might be delicate we rewrite the term (3.24) to be summed up on the right-hand side (3.23) in the form

$$\left[\ln J_l(\nu)\right]^{\overline{(3)}} = \left[\ln[1+h_l(\infty)] - h_l(\infty) + \frac{1}{2} h_l(\infty)^2\right] + h_l^{\overline{(3)}}(\infty) - \frac{1}{2} h_l^{\overline{(2)}}(\infty) \left(h_l(\infty) + h_l^{(1)}(\infty)\right) . \tag{3.25}$$

Each of the three terms on the right-hand side (RHS) is now manifestly of order V^3. The subtraction done in the large square brackets is exact enough when the logarithm is calculated with double precision.

In the numerical computation $h_l(\infty)$ is to be replaced, of course, by $h_l(r_{\max})$. We have found that $h_l(r)$ becomes constant within relative deviation of $\sim 10^{-6}$ for $r \approx (12$–$18)/m$ and we have chosen $r_{\max}$ in this range of values.

We have neglected until now the existence of the negative mode $\omega_{0,0,0}^2 < 0$ and three zero modes $\omega_{0,1,0}^2 = 0$. The former results in a negative value of $J_0(\nu) = 1 + h_0(\infty)$ at $\nu = 0$. According to Eq. (1.2) one has to replace $\omega_{0,0,0}^2$ by $|\omega_{0,0,0}^2|$. That implies taking the absolute value of $J_0(0)$ in Eq. (3.23).

The zero modes manifest themselves by the vanishing of $J_1(\nu)$ at $\nu = 0$. In the numerical calculation this zero was found at $\omega_{0,1,0}^2 \sim 10^{-5} m^2$.

It can be easily seen [7–9] that exclusion of the zero modes implies replacing $J_1(0)$ by its derivative

$$J_1'(0) = \frac{d}{d(\nu^2)} h_1(\infty) \bigg|_{\nu=0} \quad . \tag{3.26}$$

In Fig. 5 we present some results for the functions h_l. The values of the first $h_l^{(k)}(\infty)$ are plotted vs $2l+1$. For the terms summed in Eq. (3.23) we have found good agreement with the expected behavior $1/(2l+1)^4$.

B. Calculation of $\mathcal{D}^{\overline{(3)}}$

Our next step is performing summation over l in Eq. (3.23). It has been done by cutting the sum at some value $l_{\max}$ and adding the remaining sum from $l_{\max}+1$ to ∞ of terms fitted with

$$\ln J_l^{\overline{(3)}} \approx \frac{\mathrm{const}}{(2l+1)^4} + \frac{\mathrm{const}'}{(2l+1)^6} \quad . \tag{3.27}$$

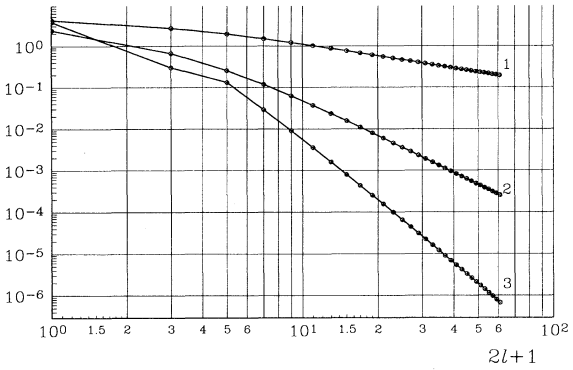

FIG. 5. The values of $J^{(k)}_{l\ \mathrm{con}}$ at $k = 1$ (curve 1), $k = 2$ (curve 2), and $J^{(3)}_{l\ \mathrm{con}}$ (curve 3) against $2l + 1$ in double logarithmic scale at $\alpha = 0$ and $\nu = 0$. The straight-line behavior at large l corresponds to the expected power law $(2l + 1)^{-2k+1}$.

The summation was stopped when increasing of $l_{\max}$ by unity did not change the result within some given accuracy δ. This happened, for example, at $l_{\max} = 12$ at $\nu = 0$, $\alpha = 0.5$. The value of δ was automatically increased during the calculation if the corresponding accuracy had not been reached.

The convergence becomes worse at higher ν or α. The reason is that the asymptotic behavior (3.27) sets in at $l \gg (\nu^2 + m^2)^{1/2} r_{\mathrm{eff}}$, where r_{eff} is the characteristic size of the bubble. It is of order $1/m$ at small values of α and can be estimated as $\{4/[3(1 - \alpha)m] + \mathrm{const}\}m^{-1}$ near the thin-wall limit $\alpha \to 1$. As the maximal value of the angular momentum that we have used is $l = 30$, the computations have been stopped somewhere at $\nu \sim 10m$.

The resulting $F^{(3)}(\nu)$ is shown in Figs. 6–8. Its magnitude at $\nu = 0$ gives the value of the infinite-temperature determinant ratio $\ln \mathcal{D}^{(3)}(\infty)$. To illustrate the efficiency of the method we note that the evaluation of $F^{(3)}(\nu)$ for

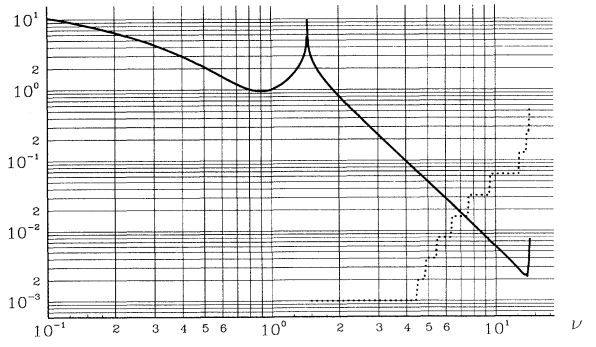

FIG. 6. Absolute value of $F^{(3)}(\nu)$ at $\alpha = 0.1$ vs $2l + 1$ in double logarithmic scale. A logarithmic singularity is seen at $\nu = \omega_-$. The actual value of $F^{(3)}(\nu)$ is negative above this point. In the region $\nu < \omega_-$ it is complex and has no physical meaning. The dotted line represents expected relative error in $F^{(3)}(\nu)$ which is estimated as 5δ (see Sec. III B).

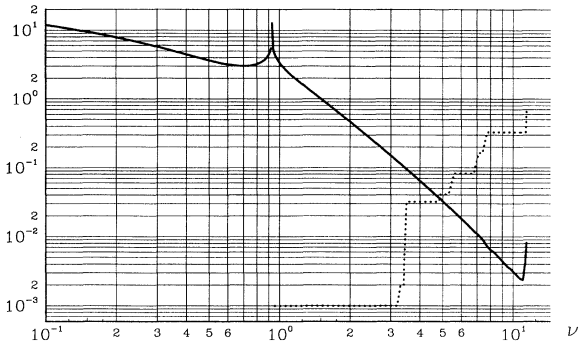

FIG. 7. The same as in Fig. 6 at $\alpha = 0.5$.

one value of ν takes typically 10–30 sec CPU time on a standard PC with a 486 processor.

The finite temperature is accounted for in $\ln \mathcal{D}^{(3)}$ which is computed according to Eq. (3.7). As $F^{(3)}(\nu) \sim 1/\nu^3$ at high ν, the summation over Matsubara frequencies is elementary.

C. Inclusion of $\mathcal{D}^{(1)}$ and $\mathcal{D}^{(2)}$

We have found the value $\ln \mathcal{D}^{(3)}$ which is the sum of all one-loop diagrams of third order and higher. Now we add to the result first- and second-order finite-temperature Feynman graphs $A^{(1)}(T)$ and $A^{(2)}(T)$ (3.20) calculated in the standard technique. It is convenient to represent both of them if the form

$$A^{(k)}(T) = \left[A^{(k)}(T) - A^{(k)}(0)\right] + A^{(k)}(0). \tag{3.28}$$

For $k = 1$ the term in square brackets is given by

$$A^{(1)}(T) - A^{(1)}(0) = \frac{1}{T}\int_0^\infty dr r^2 V(r) Q\left(\frac{m}{2T}\right) \tag{3.29}$$

with

$$Q(z) = \frac{z^2}{8\pi^2}\int_1^\infty dy \left(1 + y^2\right)^{1/2} [\coth(zy) - 1]. \tag{3.30}$$

The second order gives an UV-finite contribution to $F(\nu)$:

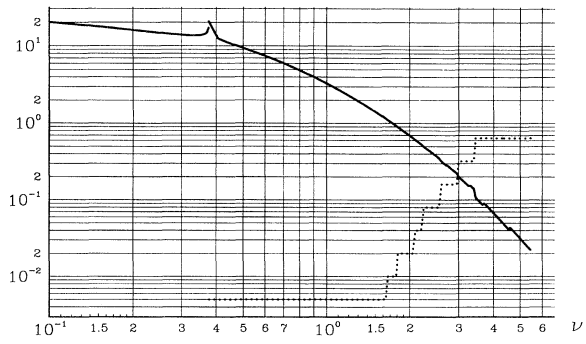

FIG. 8. The same as in Fig. 6 at $\alpha = 0.8$.

$$F^{(2)}(\nu) = -4 \int \frac{dq}{q} \arcsin\left(1 + \left(\frac{2\kappa}{q}\right)^2\right)^{-1/2} \times \left(\int_0^\infty dr r V(r) \sin qr\right)^2 . \quad (3.31)$$

We have taken $A^{(2)}(T) - A^{(2)}(0)$ (3.28) into account by calculating numerically the difference

$$A^{(2)}(T) - A^{(2)}(0) = \sum_{n=-\infty}^{\infty} F^{(2)}(2\pi n T) - \frac{1}{T}\int_{-\infty}^{\infty} \frac{d\nu}{2\pi} F^{(2)}(\nu). \quad (3.32)$$

It is sufficient to make an intermediate cutoff regularization in order to determine uniquely the difference between these two logarithmically divergent quantities.

All UV divergences have been moved now to the last terms in (3.28) which are the standard tadpole and fish diagrams at zero temperature.

To sum up, we have calculated the functional determinant (1.3) as a sum of different contributions in the following form

$$\ln\left(m^6 \mathcal{D}(T)\right) = \left[A^{(1)}(T) - A^{(1)}(0)\right] + \left[A^{(2)}(T) - A^{(2)}(0)\right] + \sum_{n=-\infty}^{\infty} F^{(3)}(2\pi n T) + A^{(1)}(0) + A^{(2)}(0) \quad . \quad (3.33)$$

Here the first term is given by Eq. (3.29), the second one is defined in (3.32) and (3.31), the sum of $F^{(3)}$ has been calculated numerically, and two last terms are usual zero-temperature Feynman diagrams (3.20) in the external potential V.

$A^{(1)}(0)$ and $A^{(2)}(0)$ contain now all the ultraviolet divergences and have to be regularized. The cutoff dependence introduced thereby disappears, however, in the full one-loop contribution to the effective action

$$S_{\text{one loop}} = \frac{1}{2}\ln[m^6 \mathcal{D}(T)] + S_{\text{ct}} \quad (3.34)$$

that enters the formula for the transition rate (1.2). In the model considered here S_{ct} has the form

$$S_{\text{ct}} = \int d^4x \left(\epsilon\varphi + \frac{1}{2}\delta m^2 \varphi^2 - \delta\eta\varphi^3 + \frac{1}{8}\delta\lambda\varphi^4\right). \quad (3.35)$$

A possible scheme for fixing the counterterms is deferred to the next section.

IV. A POSSIBLE RENORMALIZATION

While renormalization requires just standard techniques it is not straightforward here to select a specific renormalization prescription because the scheme depends strongly on the physical context in which the first-order phase transition is considered. Though we consider Eq. (3.33) in its general form as our main result, we would like to discuss now a possible scheme of fixing the counterterms.

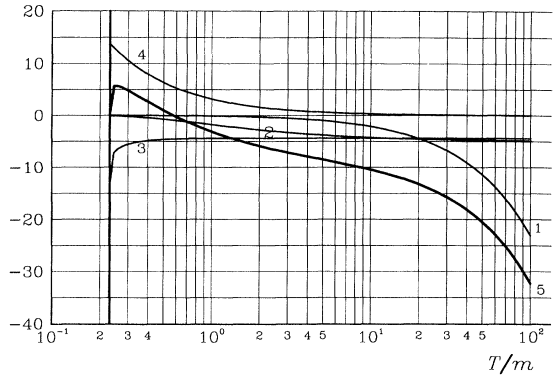

FIG. 9. The value of $S_{\text{one loop}}$ (3.34) at $\alpha = 0.1$ vs T/m: Curves 1–3 correspond to the first, second, and third terms on the RHS of (3.33). The fourth one represents the sum of the last two terms in (3.33) and S_{ct}, (3.35) and (4.1). This contribution depends on temperature via the factor $1/T$ only. Curve 5 displays the full result $S_{\text{one loop}}$. The temperature range is bounded from the left by $T_{\min} = 0.2301m$ where the result has a logarithmic singularity.

The scheme is chosen in the spirit of renormalization suitable in consideration of the electroweak cosmological phase transition. As the latter is tightly connected with particle physics, it is appropriate to fix the mass and the vacuum expectation value of the scalar field. This implies the following conditions on the temperature-dependent effective potential $U_{\text{eff}}(\varphi; T)$ and the one-loop Euclidean propagator in the true vacuum $D_+(p^2)$:

$$\begin{aligned} &D_+(-m_+^2) = 0, \\ &U'_{\text{eff}}(\phi_+; 0) = 0, \\ &U'_{\text{eff}}(0; 0) = 0, \\ &U_{\text{eff}}(\phi_+; 0) = U(\phi_+), \end{aligned} \quad (4.1)$$

where m_+^2 stands for the particle mass in the true vacuum. The last two conditions set the false vacuum to be

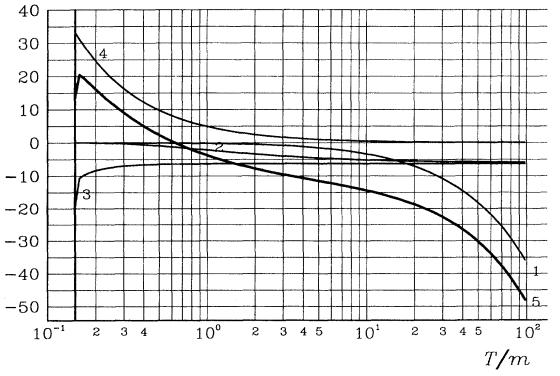

FIG. 10. The same as in Fig. 9 at $\alpha = 0.5$; here $T_{\min} = 0.148m$.

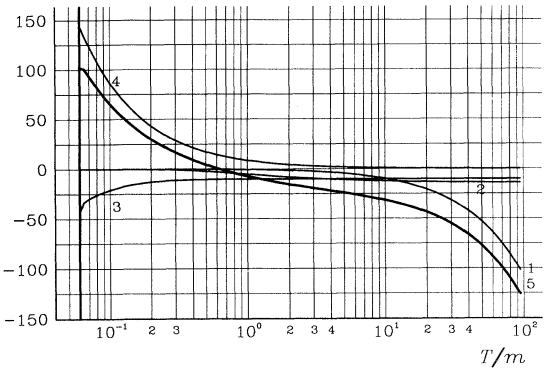

FIG. 11. The same as in Fig. 9 at $\alpha = 0.8$; here $T_{\min} = 0.0598m$.

at $\varphi = 0$ and fix the density of energy stored in it. They are more specific for our toy model.

In addition to Eqs. (4.1) one has to solve one more system of equations

$$\begin{aligned} \frac{1}{2}m^2\phi_+^2 - \eta\phi_+^3 + \frac{1}{8}\lambda\phi_+^4 &= U(\phi_+), \\ m^2 - 3\eta\phi_+ + \frac{1}{2}\lambda\phi_+^2 &= 0, \\ m^2 - 6\eta\phi_+ + \frac{3}{2}\lambda\phi_+^2 &= 0, \end{aligned} \tag{4.2}$$

in order to express m^2, η, and λ in the classical bubble energy (2.2) and (2.3) in terms of m_+^2, ϕ_+, and $U(\phi_+)$.

The results of the application of this renormalization scheme are plotted in Figs. 9–11. We note that the temperature appears neither in the field potential (2.1) nor in the renormalization conditions (4.1). All finite-temperature corrections are therefore contained in the fluctuation determinant. This results in a linear temperature dependence due to the first term in (3.33). Thus, our simple one-loop approximation fails at very high temperature. It is not valid also at $\alpha \to 0$ due to the high difference of the mass scales of states built on the false and true vacua. This manifests itself by a logarithmically large contribution appearing in $S_{\rm ct}$ (3.35).

V. DISCUSSION AND CONCLUSION

The model considered here is only semirealistic. Nevertheless we would like to add some remarks on our results. We find that the correction to the bubble nucleation rate (1.2) coming from diagrams of the third order and higher favors the transition (i.e., $\ln \mathcal{D}^{(3)} < 0$). The sign of the full one-loop contribution to the effective action $S_{\text{one loop}}$ depends on the renormalization scheme. With our choice (4.1) it enhances $\gamma(T)$ at high temperature due to the tadpole diagram (3.29). This contribution becomes too big at $T \gg m$ and then the naive application of the one-loop approximation becomes inconsistent. This is a manifestation of the known problem of relating the parameters of the theory at zero and very high temperatures. Another feature of our results (Figs. 9–11) is a weak logarithmic singularity at $T = T_{\min}$, the temperature at which one more fluctuation mode of the critical bubble becomes unstable. Numerically it is unimportant. Moreover, in a finite region of temperature $T_{\min} < T < T_{\text{tunn}}$ quantum tunneling has to be taken into consideration.

We have developed here a method for calculating functional determinants and have tested it under realistic conditions. In particular we have shown that within this formalism the problems connected with ultraviolet divergences, zero and unstable modes can be handled easily and without loss of numerical accuracy. Moreover the algorithm is so fast that the whole calculation presented here can be performed on a standard PC with a 486 processor within 1 h for one value of α. The extension of the method to more complex gauge and fermionic systems is straightforward once the fluctuation equations are known [12, 13].

ACKNOWLEDGMENT

The work of V.G.K. was supported by the Alexander von Humboldt Foundation and, in its initial stage, by the Byelorussian Foundation for Fundamental Research, Grant No. Φ2-23.

[1] J. S. Langer, Ann. Phys. (N.Y.) **41**, 108 (1967).
[2] J. S. Langer, Ann. Phys. (N.Y.) **54**, 258 (1969).
[3] S. Coleman, Phys. Rev. D **15**, 2929 (1977).
[4] C. G. Callan and S. Coleman, Phys. Rev. D **16**, 1762 (1977).
[5] R. F. Dashen, B. Hasslacher, and A. Neveu, Phys. Rev. D **10**, 4114 (1974); I. M. Gel'fand and A. M. Yaglom, J. Math. Phys. **1**, 48 (1960); R. H. Cameron and W. T. Martin, Bull. Am. Math. Soc. **51**, 73 (1945); J. H. van Vleck, Proc. Natl. Acad. Sci. **14**, 178 (1928).
[6] S. Coleman, in *The Whys of Subnuclear Physics*, Proceedings of the International School, Erice, Italy, 1977, edited by A. Zichichi, Subnuclear Series Vol. 15 (Plenum, New York, 1979).
[7] V. G. Kiselev and K. G. Selivanov, Pis'ma Zh. Eksp. Teor. Fiz. **39**, 72 (1984) [JETP Lett. **39**, 85 (1984)].
[8] V. G. Kiselev and K. G. Selivanov, Yad. Fiz. **43**, 239 (1986) [Sov. J. Nucl. Phys. **43**, 153 (1986)].
[9] K. G. Selivanov, Zh. Eksp. Teor. Fiz. **94**, 57 (1988) [Sov. Phys. JETP **67**, 1548 (1988)].
[10] M. Dine, R. G. Leigh, P. Huet A. Linde, and D. Linde, Phys. Rev. D **46**, 550 (1992); Phys. Lett. B **283**, 319 (1992).
[11] J. Baacke, Acta Phys. Pol. B **22**, 127 (1991), and references therein.
[12] J. Baacke, Z. Phys. C **53**, 402 (1992).
[13] J. Baacke and S. Junker, Report No. DO-TH-93/19, Dortmund University, 1993 (unpublished).